IJAO
ISSN 0391-3988

Int J Artif Organs 2016; 39(1): 28-36
DOI: 10.5301/ijao.5000469

ORIGINAL ARTICLE

Morphometric analysis of the infraorbital foramen, canal and groove using cone beam CT: considerations for creating artificial organs

Kaan Orhan[1], Melis Misirli[2], Secil Aksoy[2], Umut Seki[1] Evren Hincal[3], Tugrul Ormeci[4], Ahmet Arslan[5]

[1] Ankara University, Faculty of Dentistry, Department of Dentomaxillofacial Radiology, Ankara - Turkey
[2] Near East University, Faculty of Dentistry, Department of Dentomaxillofacial Radiology, Mersin - Turkey
[3] Near East University, Faculty of Arts & Sciences, Department of Mathematics, Mersin - Turkey
[4] Medipol University, Faculty of Medicine, Department of Radiology, Istanbul - Turkey
[5] Yeditepe University, Faculty of Dentistry, Department of Oral and Maxillofacial Surgery, Istanbul - Turkey

ABSTRACT

Purpose: The aim of this study was to examine the anatomy and variations of the infraorbital foramen and its surroundings via morphometric measurements using cone beam computed tomography (CBCT) scans derived from a 3D volumetric rendering program.

Methods: 354 sides of CBCT scans from 177 patients were examined in this study. DICOM data from these images were exported to Maxilim® software in order to generate 3D surface models. The morphometric measurements were done for infraorbital foramen (IOF), infraorbital groove (IOG) and infraorbital canal (IOC). All images were evaluated by 1 radiologist. To assess intra-observer reliability, the Wilcoxon matched-pairs signed rank test was used. Differences between sex, side, age and measurements were evaluated using chi-square and paired *t*-test and measurements were evaluated using 1-way ANOVA tests. Differences were considered significant when $p<0.05$.

Results: The most common shape was oval for IOF and parallel for IOC without any accessory foramen. The results showed that females have smaller dimensions for the measurements between the two foramen rotundum (FR), FR-IOF, sella-FR, center of the IOF (cIOF)-nasion (N), cIOF-NB (nasion-B) ($p>0.05$). No significant difference was found according to age groups ($p>0.05$).

Conclusions: These results provide detailed knowledge of the anatomical characteristics in this particular area. CBCT imaging with lower radiation dose and thin slices can be a powerful tool for anesthesia procedures like infra orbital nerve blocks, for surgical approaches like osteotomies and neurectomies and also for generating artificial prostheses.

Keywords: Anatomical models, Anatomy, Cone beam computed tomography, Infraorbital foramen, Morphometric measurements, Surgical models

Introduction

The infraorbital foramen (IOF) is one of the most important facial foramens, and the infraorbital nerve emerges from the IOF and the branches to innervate the middle region of the face. The infraorbital canal (IOC) is located in the orbital part of maxilla and shows the upward and lateral course. It opens via the IOF just below the margin of orbit (1). The infraorbital groove (IOG) branches from the inferior orbital fissure and is formed by the orbital floor of maxilla. These structures allow passage of the infraorbital vessels and nerve (2). The infraorbital nerve (ION) is the continuation of the maxillary nerve, which is responsible for sensory innervation to the skin of malar area between the lower eyelid and upper lip. The IOF is important anatomically in the infraorbital nerve block, especially in regional anesthesia for the treatment of pathological conditions like cyst enucleation, for cleft palate and lip surgery, endoscopic sinus surgery in infants, and radiofrequency ablation of trigeminal ganglion in trigeminal neuralgia for elderly patients (3, 4). Beyond these therapies, in cases when the dissection of the periosteum of the face is performed, such as in maxillary osteotomies or midfacial lift surgeries for the correction of midfacial ptosis, surgeons must be careful of the location of the IOF (5, 6).

The use of cone-beam computed tomography (CBCT) was first reported by Mozzo et al (7) and has been proposed in the last decade for maxillofacial imaging (8, 9). A CBCT scan uses

Accepted: January 26, 2016
Published online: February 9, 2016

Corresponding author:
Dr. Kaan Orhan
Ankara University
Faculty of Dentistry
Department of Dentomaxillofacial Radiology
Ankara, Turkey
call53@yahoo.com

a different type of acquisition than that used in multislice CT (MSCT). Rather than capturing an image as separate slices as in MDCT, CBCT produces a cone-shaped X-ray beam that allows an image to be captured in a single shot. The resultant volume can be reformatted to provide multiple reconstructed images (e.g., sagittal, coronal, and axial) that are similar to traditional MDCT images (10, 11). CBCT thus offers the distinct advantage of a lower radiation dose than MDCT and the possibility of importing and exporting individualized, overlap-free reconstructions. Moreover, these possibilities and increasing access to CBCT imaging for surgeons and are enabling the movement from 2D analysis to 3D analysis prior to all kinds of surgeries. Studies of CBCT applications in maxillofacial surgery have shown it to be a reliable and accurate tool for linear and 3D measurements prior to surgery (12).,

New technologies like CBCT-based models help to understand the anatomy and pathology of the hard tissues in living subjects. This innovative method reduces errors and contributes to the development of new imaging markers for risk factors (13). Gomez et al (14) developed computed tomography based models for assessing condylar morphology and reported that the 3D surface models constructed from CBCT images are comparable to those derived from MSCT scans. He also reported that CBCT is a reliable tool for considering condylar morphology.

Many anatomical studies of this region using cadavers have been reported in the literature in English (15-19), but to the best of our knowledge there is no study that comparatively evaluates the anatomy of the IOF, IOC, IOG and their relations with neighborhood anatomical structures using CBCT imaging. It was therefore considered worthwhile to examine the anatomy and variations of the infraorbital foramen and its surroundings via morphometric measurements using cone beam CT scans derived from a volumetric rendering software.

Materials and methods

Data from CBCT examinations of 354 sites in 177 patients who had been referred to our outpatient clinic during a 5-year period were analyzed retrospectively. The overall mean age was 38.4 years (range: 18-70 years, standard deviation (SD): 16.7 years). Informed consent was obtained from all patients before CBCT examinations. The mean age of the male patients was 39.2 (SD, 17.66; n = 86) years (range, 18-69 years), while the mean age of the female patients was 37.6 (SD, 15.63; n = 91) years (range, 18-70 years).

Patients with evidence of bone disease (especially osteoporosis), relevant drug consumption, skeletal asymmetries or trauma, congenital disorders, anamnesis of surgical procedures in the TMJ, and pathological disorders of the maxilla and mandible as well as syndromic patients were excluded from the study. The study protocol was carried out according to the principles described in the Declaration of Helsinki, including all amendments and revisions. Only the investigators had access to the collected data. The institutional review board of the faculty reviewed and approved informed consent forms. There was no preference for gender regarding sample choice. Only high-quality scans were included. Low-quality images, such as those containing scattering or insufficient accuracy of bony borders, were excluded. Patients were grouped according to gender and age groups: 18 to 25, 26 to 50, and 50 and over.

Imaging using CBCT

CBCT scans were obtained using a Newtom 3G (Quantitative Radiology). All CBCT scans were obtained according to the strict, standardized scanning protocol used in our clinic. Patients were placed in a horizontal position, checked to ensure that their mouths were closed in a normal, natural occlusive position and instructed to lie still throughout the length of the scan. Images were obtained using a 9-inch (0.25 mm^3) or 12-inch (0.40 mm^3) field of view (to ensure inclusion of the entire facial anatomy), 0.3 mm-thick axial slices and isotropic voxels. Axial images were exported in a DICOM file format with a 512 × 512 matrix and imported to Maxilim® (version 2.3.0; Medicim). The anatomical and morphometric evaluations and measurements were done by means of this software.

All images were reconstructed on a 21.3-inch, flat-panel, color active matrix TFT medical display (Nio Color 3MP; Barco) with a resolution 76 Hz, 0.2115-mm pitch 10 bit. The examiners were also permitted to use enhancements and orientation tools such as magnification, brightness, and contrast to improve visualization of the landmarks.

Image evaluation

All CBCT images were retrospectively evaluated by a dentomaxillofacial radiologist with 12 years of experience (K.O.). Image evaluations were done in sagittal and coronal CBCT slices together with superimposition of 3D skull representations (Fig. 1).

On both sides, the size of the IOF was measured horizontally and vertically on X (the width) and Y axis (the height). The horizontal plane was defined as the plane that was parallel to the nasal floor and passed through the IOF; the vertical plane was defined as the plane that was parallel to the sagittal plane and passed through the IOF (Fig. 1).

Besides the size, the shape of the IOF (oval or rounded), the shape of the IOC (parallel or hourglass), the presence of accessory IOF, the angle between the N (nasion)-IOF-S (sella), the angle between the N-S-IOF (Fig. 2), the distance between the foramen rotundum (FR)-IOF, the distance between FR- (inferior orbital fissure) (InfOF), the distance between IOF-IOF, S-center of IOF (cIOF), cIOF-N, InfOF-IOF, InfOF- (infraorbital margin) (IOM), cIOF- (the lateral process of the canine tooth) (CT), the distance between the upper pole of the IOF (uIOF)-IOM, cIOF-NB, the length of the IOC, the length of the IOM were measured on both sides (Figs. 2 and 3).

The length of the IOC was defined as the distance from the center of the IOF to the portion where the axis of the IOC changed. The length of the IOG was defined as the sum of the IOG uncovered by the bone and portion that was parallel to the orbital floor and covered by the bone. In addition to these measurements, ANS-NB, FR-FR, N-ANS, S-FR and S-N were all measured on both sides (Fig. 4).

Statistical analyses were performed using IBM SPSS software (version 20.0.1). Wilcoxon matched-pair, signed-rank tests were used to assess the intra-observer reliability of

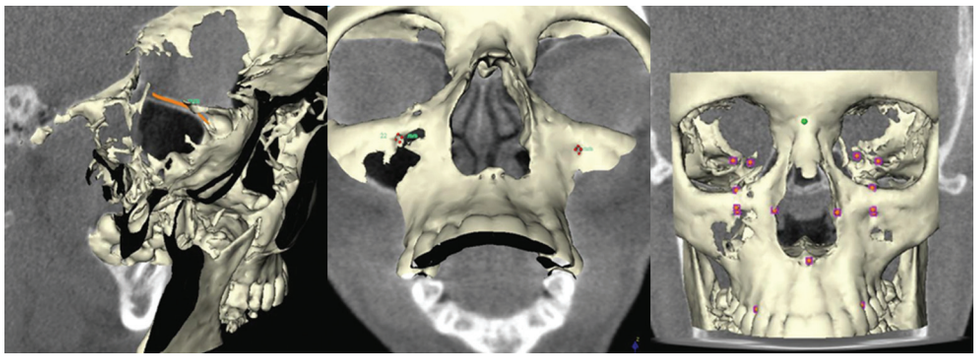

Fig. 1 - General layout of the Maxilim® software showing hard-tissue segmentation together with radiographic slices in sagittal and coronal CBCT views together with superimposition of 3D skull representations.

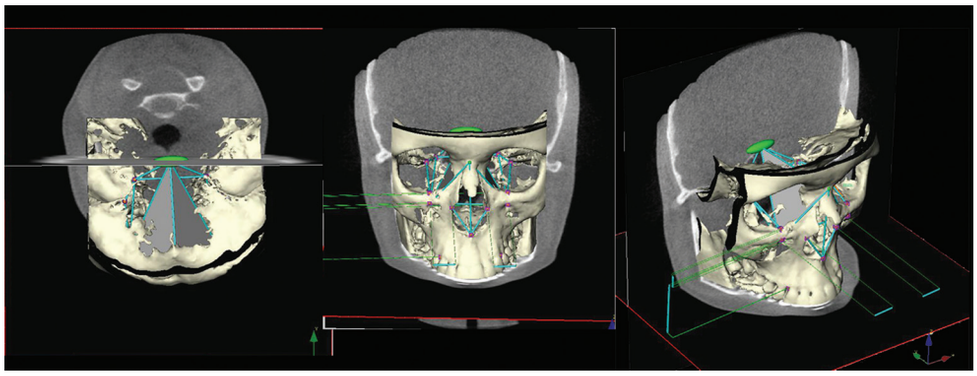

Fig. 2 - Figure showing all measurements [the size, the shape of infraorbital foramen (IOF) (oval or rounded), the shape of IOC (parallel or hourglass)], the presence of accessory IOF, the angle between the [N (nasion)-IOF-S (sella), the angle between the N-S-IOF] that was performed in the study.

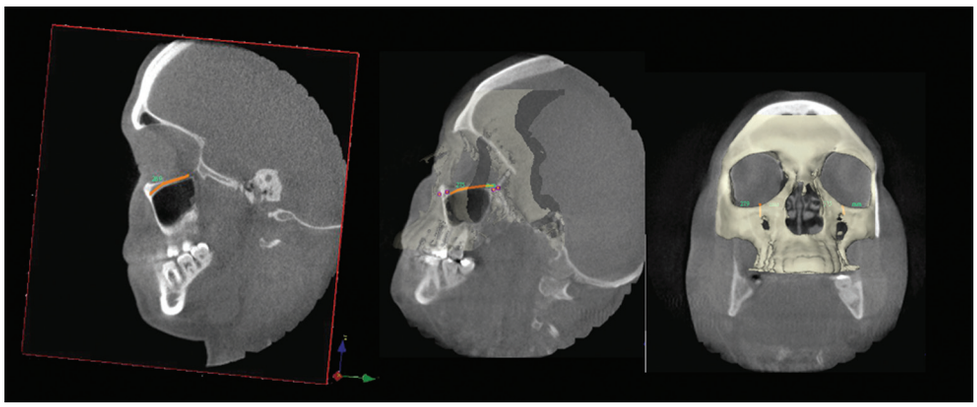

Fig. 3 - Figure showing the measurement of the infraorbital canal (IOC) in different slices.

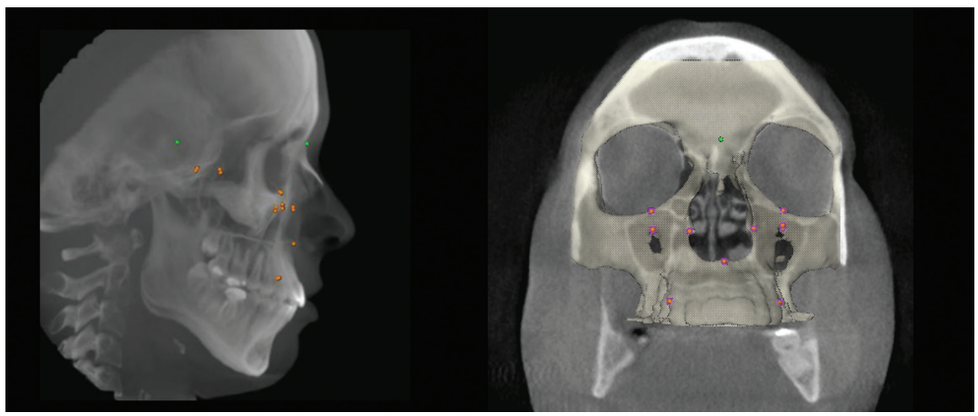

Fig. 4 - Figure showing the measurements of the infraorbital canal (IOC), infraorbital grove (IOG), anterior nasal spine- NB line (ANS-NB), Frankfort horizontal plane (FR-FR), nasion-anterior nasal spine (N-ANS), S (sella)-FR and SN landmarks.

repeated measurements and examinations. Differences between sex, side, age and measurements were evaluated using chi-square and paired *t*-test and measurements were evaluated using 1-way ANOVA tests. Differences were considered significant when p<0.05.

Results

Repeated measurements of CBCTs showed no significant intra-observer difference (p>0.05). Overall, intra-observer consistency was 94.2% between 2 measurements. All measurements were found to be highly reproducible. The average of the measurements was constituted as final data for the study.

The horizontal (x axis) and the vertical (y axis) measurements are presented in Table I. Although no statistically significant difference was observed between males and females, the size of IOF was always bigger in males (p>0.05). Table II shows the shape of the IOF and IOC for left and right sides. Examination of the 354 sides of the 177 CBCT scans revealed that the most common shape was oval for the IOF, parallel for the IOC and there was no accessory foramen. In addition, no statistically significant difference was observed between the genders on both sides (p>0.05).

The measurement between ANS-NB, FR-FR, FR-IOF, IOF-IOF, N-ANS, S-FR, S-N, S-cIOF, cIOF-N, InfOF-IOF, InfOF-IOM, cIOF-CT, cIOF-NB, IOC length and IOG length were all significantly greater in males (Tab. III). In all cases the average of the IOC length on the right side was determined to be significantly higher compared to the left side (p = 0.029; p<0.05). In all males, the average length of the IOC obtained on the right side was higher compared to the left side (p = 0.049; p<0.05).

Table IV shows the width of the IOF on the X axis and the height of the IOF on the Y axis according to age groups. No statistically significant difference was noticed between young and older ones. Table V shows the shape of the IOF, either round or oval, according to same age groups. It also shows the shape of the optic canal either sand glass or parallel. No statistically significant difference was obtained regarding the shape of the optic canal and the IOF.

TABLE I - Measurements of the infraorbital foramen (IOF) on the x axis (width) and y axis (height) in different sexes

		Total n = 177	Male n = 86	Female n = 91	p[1]
		Mean ± SD	Mean ± SD	Mean ± SD	
IOF Right X Axis		3.52 ± 0.81	3.53 ± 0.75	3.51 ± 0.78	0.076
IOF Left X Axis		3.66 ± 0.88	3.86 ± 0.91	3.46 ± 0.79	0.595
	p[2]	0.776	0.218	0.237	
IOF Right Y Axis		4.84 ± 1.21	5.10 ± 1.44	4.58 ± 1.11	0.079
IOF Left Y Axis		4.82 ± 1.29	5.05 ± 1.38	4.59 ± 1.13	0.492
	p[2]	0.760	0.296	0.786	

[1] Student's *t*-test.
[2] Paired sample *t*-test; *p<0.05.

TABLE II - Determination of the shape of the infraorbital foramen (IOF) and the infraorbital canal (IOC) in different sexes

		Male n = 86	Female n = 91	Total n = 177	p
	Shape	n%	n%	n%	
IOF Right	Rounded	32 (37.5%)	14 (15.4%)	46 (26%)	0.145
	Ovale	54 (62.5%)	77 (84.6%)	131 (74%)	
IOF Left	Rounded	32 (37.5%)	14 (15.4%)	46 (26%)	0.145
	Ovale	54 (62.5%)	77 (84.6%)	131 (74%)	
IOC Right	Sandglass	17 (20.8%)	11 (11.5%)	28 (16%)	0.456
	Parallel	69 (79.2%)	80 (88.5%)	149 (84%)	
IOC Left	Sandglass	14 (16.7%)	11 (11.5%)	25 (14%)	0.697
	Parallel	64 (83.3%)	80 (88.5%)	152 (86%)	

IOC = infraorbital canal.

TABLE III - Measurements of the infraorbital foramen (IOF) and several anatomic landmarks around the IOF

		Gender			p[1]
		Total n = 177	Male n = 86	Female n = 91	
		Mean ± SD	Mean ± SD	Mean ± SD	
Right N-IOF-S		73.1 ± 3.94	73.71 ± 4.26	72.53 ± 3.61	0.292
Left N-IOF-S		72.78 ± 3.82	73.04 ± 3.94	72.54 ± 3.76	0.649
	p[2]	0.312	0.143	0.971	
Right N-S-IOF		40.41 ± 3.89	39.83 ± 4.17	40.96 ± 3.6	0.308
Left N-S-IOF		40.32 ± 3.55	39.84 ± 3.9	40.77 ± 3.22	0.362
	p[2]	0.704	0.974	0.55	
Right ANS-NB		21.18 ± 2.89	22.3 ± 3.15	20.15 ± 2.23	0.008**
Left ANS-NB		20.97 ± 2.93	22.33 ± 3.04	19.71 ± 2.2	0.001**
	p[2]	0.168	0.891	0.048*	
FR-FR		39.75 ± 3.11	40.98 ± 3.13	38.62 ± 2.67	0.006**
Right FR-IOF		44.84 ± 3.61	46.33 ± 4.05	43.46 ± 2.52	0.005**
Left FR-IOF		45.25 ± 3.65	46.4 ± 4.24	44.19 ± 2.68	0.035*
	p[2]	0.148	0.876	0.044*	
Right FR-InfOF		16.79 ± 3.27	16.77 ± 3.33	16.82 ± 3.28	0.962
Left FR-InfOF		17.01 ± 3.83	16.89 ± 4.07	17.13 ± 3.66	0.828
	p[2]	0.659	0.82	0.71	
IOF-IOF		51.53 ± 3.93	53.01 ± 4.53	50.17 ± 2.72	0.011*
N-ANS		52.7 ± 3.84	54.47 ± 3.76	51.07 ± 3.18	0.001**
Right S-FR		26.31 ± 1.99	27.03 ± 2.05	25.65 ± 1.73	0.014*
Left S-FR		26.36 ± 3.27	27.77 ± 3.68	25.05 ± 2.2	0.002**
	p[2]	0.899	0.218	0.087	
S-N		68.18 ± 3.96	70.44 ± 3.7	66.1 ± 2.96	0.001**
Right S-cIOF		65.39 ± 4.02	67.36 ± 3.95	63.57 ± 3.18	0.001**
Left S-cIOF		65.7 ± 4.62	67.92 ± 4.85	63.65 ± 3.34	0.001**
	p[2]	0.18	0.119	0.778	
Right cIOF-N		46.11 ± 3.27	46.91 ± 3.47	45.38 ± 2.95	0.042*
Left cIOF-N		46.11 ± 3	47.08 ± 3.33	45.21 ± 2.39	0.026*
	p[2]	0.982	0.702	0.617	
Right InfOF-IOF		31.73 ± 3.81	33.16 ± 4.02	30.4 ± 3.11	0.009**
Left InfOF-IOF		31.58 ± 3.87	32.53 ± 4	30.71 ± 3.6	0.008**
	p[2]	0.751	0.298	0.645	
Right InfOF-IOM		30.76 ± 3.51	32.03 ± 3.54	29.59 ± 3.09	0.012*
Left InfOF-IOM		30.37 ± 3.16	31.5 ± 2.97	29.32 ± 3.02	0.013*
	p[2]	0.32	0.309	0.658	
Right cIOF-CT		33.61 ± 3.59	35.19 ± 3.53	32.15 ± 3.02	0.002**
Left cIOF-CT		33.39 ± 3.85	34.98 ± 3.76	31.92 ± 3.38	0.004**
	p[2]	0.311	0.484	0.476	
Right uIOF-IOM		7.43 ± 1.87	7.74 ± 2.06	7.14 ± 1.66	0.262
Left uIOF-IOM		7.66 ± 1.79	7.7 ± 1.96	7.62 ± 1.65	0.875
	p[2]	0.187	0.906	0.005**	
Right cIOF-NB		13.83 ± 1.71	14.16 ± 1.75	13.52 ± 1.63	0.018*
Left cIOF-NB		13.87 ± 1.89	14.51 ± 2.03	13.27 ± 1.57	0.020*
	p[2]	0.886	0.309	0.502	
Right IOC Length		28.32 ± 3.85	29.81 ± 4.34	26.93 ± 2.75	0.007**
Left IOC Length		27.46 ± 4.27	28.88 ± 4.67	26.14 ± 3.46	0.022*
	p[2]	0.029*	0.049*	0.209	
Right IOG Length		3.52 ± 0.97	3.72 ± 1.12	3.63 ± 0.84	0.040*
Left IOG Length		3.46 ± 0.79	3.73 ± 0.79	3.22 ± 0.71	0.021*
	p[2]	0.613	0.302	0.016*	

[1] Student's *t*-test.
[2] Paired sample *t*-test.
* p<0.05.
** p<0.01.

TABLE IV - Measurements of the infraorbital foramen (IOF) on the x axis (width) and y axis (height) in different age groups

	Age Groups			p
	18-25	26-50	50<	
	Mean ± SD	Mean ± SD	Mean ± SD	
Infraorbital foramen Right X axis	3.46 ± 0.62	3.57 ± 1.06	3.53 ± 1.25	0.319
Infraorbital foramen Right Y axis	4.85 ± 0.99	4.80 ± 1.08	4.87 ± 1.35	0.374
Infraorbital foramen Left X axis	3.57 ± 0.84	3.74 ± 0.82	3.67 ± 0.73	0.344
Infraorbital foramen Left Y axis	4.72 ± 1.11	4.91 ± 1.52	4.81 ± 1.87	0.923

Number of males = 86; number of females = 91.

TABLE V - Determination of the shape of the infraorbital foramen (IOF) and optic canal in different age groups

	Shape	Age groups			p
		18-25	26-50	50 <	
		n (%)	n (%)	n (%)	
IOF Right	Round	21 (27.3%)	14 (22.2%)	11 (30%)	0.889
	Ovale	57 (72.7%)	49 (77.8%)	25 (70%)	
IOF Left	Round	17 (22.7%)	14 (22.2%)	14 (40%)	0.529
	Ovale	61 (77.3%)	49 (77.8%)	22 (60%)	
Optic Canal Right	Hour glass	14 (18.2%)	31 (5.6%)	11 (30%)	0.223
	Parallel	64 (%81.8)	32 (%94.4)	25 (%70)	
Optic Canal Left	Hour glass	11 (%13.6)	7 (%11.1)	7 (%20)	0.808
	Parallel	67 (%86.4)	56 (%88.9)	29 (%80)	

Number of males = 86; number of females = 91.

Table VI shows the measurements of neighborhood anatomical region of the IOF between the right and left sides and also the measurement of the FR-FR, IOF-IOF, N-ANS, S-N according to age groups. No statistically significant difference was observed on the left side of the ANS-NB and N-ANS in both measurements between the age groups ($p>0.05$).

Discussion

CT and CBCT modalities that have come into use over the past decade have been found to overcome the limitations in surgical procedures. As a result of technological advances in the imaging, the CBCT 3D imaging technique has become used routinely especially for ENT (Ear-nose-throat) and maxillofacial presurgical imaging purposes (9, 11). In general, CBCT has been recommended as a dose-sparing technique, compared with standard medical CT scans, for the imaging of anatomical landmarks before surgical procedures. The effective dose (ICRP 2007) (International commission on radiological protection) from a standard dental protocol scan using a traditional CT was 1.5 to 12.3 times greater than comparable medium-FOV dental CBCT scans. CBCT image quality has also been found to be equivalent to that of traditional CT for visualizing the maxillofacial structures (12, 20, 21).

CBCT has a revolutionary role in the diagnosis and treatment planning of craniofacial disorders. The lower radiation dose and cost compared with MSCT provide clinicians with a valuable diagnostic tool for identifying specific changes in the morphology of craniofacial regions like the mandibular condyles with osteoarthritis (22). CBCT-based, 3D surface models provide additional diagnostic information on size, shape and the exact location of the bone abnormality of the affected joint (14).

Determination of IOF is important for percutaneous interventions. Although it is important to palpate and identify the location of IOF under soft tissue and skin, the knowledge of the position of the IOF and related structures such as the IOC and the IOG is useful for a safe block of the infraorbitalis nerve. Recently, a CT-based, 3D reconstruction method has made it possible to measure the lengths and angles of various structures in the craniofacial bone with certain software. The reliability and accuracy of this method has been proved by previous studies (10, 23). After identifying anatomical landmarks around the IOF, we made necessary measurements on 3D models between these landmarks.

TABLE VI - Measurements of the infraorbital foramen (IOF) and several anatomic landmarks around the IOF in different age groups

		Age Groups			p
		18-25	26-50	50<	
		n (%)	n (%)	n (%)	
N-IOF-S	Right	73.15 ± 4.32	73.32 ± 3.75	72.57 ± 3.73	0.891
	Left	72.52 ± 3.69	73.09 ± 4.39	72.8 ± 3.28	0.900
N-S-IOF	Right	40.04 ± 3.91	40.42 ± 3.46	41.23 ± 4.79	0.731
	Left	39.89 ± 3.92	40.26 ± 2.41	41.39 ± 4.5	0.547
ANS-NB	Right	20.22 ± 2.83	21.59 ± 2.61	22.54 ± 3.05	0.080
	Left	19.93 ± 2.75	21.34 ± 2.66	22.58 ± 3.16	0.084
FR-FR		39.48 ± 2.74	39.86 ± 3.96	40.15 ± 2.27	0.844
FR-IOF	Right	44.62 ± 3.38	45.08 ± 4.42	44.88 ± 2.7	0.925
	Left	45.16 ± 3.06	45.54 ± 4.24	44.92 ± 4.06	0.905
FR-infOF	Right	16.49 ± 3.47	17.8 ± 3.04	15.65 ± 2.99	0.214
	Left	16.67 ± 4.28	17.54 ± 3.49	16.81 ± 3.62	0.770
IOF-IOF		50.54 ± 3.39	52.57 ± 4.06	51.84 ± 4.64	0.260
N-ANS		51.37 ± 2.86	53.16 ± 4.69	54.8 ± 3.16	0.049*
S-FR	Right	26.01 ± 1.78	26.63 ± 2.47	26.41 ± 1.53	0.621
	Left	26.33 ± 2.96	26.59 ± 4.2	25.99 ± 2.07	0.901
S-N		67.88 ± 4.88	68.83 ± 3.21	67.68 ± 3.03	0.687
S-cIOF	Right	65.2 ± 4.35	65.84 ± 4.14	64.97 ± 3.27	0.833
	Left	65.8 ± 5.12	66.16 ± 4.7	64.66 ± 3.44	0.716
cIOF-N	Right	45.48 ± 2.68	46.57 ± 3.12	46.69 ± 4.62	0.482
	Left	45.45 ± 2.69	46.57 ± 2.85	46.73 ± 3.87	0.393
infOF-IOF	Right	31.85 ± 4.16	31.24 ± 3.83	32.32 ± 3.14	0.765
	Left	32.1 ± 4.45	31.5 ± 3.52	30.59 ± 3.16	0.598
infOF-IOM	Right	30.81 ± 3.59	30.18 ± 3.42	31.7 ± 3.62	0.556
	Left	30.51 ± 3.54	30.27 ± 3.2	30.23 ± 2.43	0.963
cIOF-CT	Right	32.57 ± 3.3	34.05 ± 4.23	35.09 ± 2.33	0.149
	Left	32.25 ± 3.44	33.91 ± 4.62	34.96 ± 2.56	0.141
uIOF-IOM	Right	7.64 ± 1.81	7.64 ± 1.81	6.58 ± 2.05	0.280
	Left	7.92 ± 1.54	7.82 ± 1.76	6.82 ± 2.23	0.250
cIOF-NB	Right	13.53 ± 1.57	14.19 ± 1.86	13.84 ± 1.74	0.489
	Left	14.06 ± 1.98	13.76 ± 2.05	13.63 ± 1.48	0.803
Lenght of IOC	Right	28.01 ± 4.35	28.29 ± 3.37	29.04 ± 3.77	0.788
	Left	27.49 ± 4.74	27.59 ± 4.1	27.14 ± 3.84	0.965
Lenght of IOG	Right	3.58 ± 1.1	3.55 ± 0.84	3.35 ± 0.97	0.826
	Left	3.41 ± 0.83	3.34 ± 0.63	3.78 ± 0.94	0.353

Number of males = 86; number of females = 91.

First of all, if a surgeon wants to perform an ION (infraorbital nerve) block or neurectomy, he or she must be aware of the location, slope of the canal and number of the foramina. Aggarwall et al (24) examined 67 dried, intact, adult skulls and stated that 21% of them contained multiple foramina. In the present study, all subjects appeared with only 1 single infraorbital foramen on each side of their skull. Regarding the slope of the canal, the surgeon must insert the needle upward and laterally (25). As already known, the IOC continues in the IOG located in the orbital floor; the tip of the needle must not be placed too posteriorly to avoid damaging the orbital structures or pterygopalatine fossa. In the present study, the average length of the IOC was found to be 29.81 ± 4.34 (right side for males), 28.88 ± 4.67 (left side for males), 26.93

± 2.75 (right side for females) and 26.14 ± 3.46 (left side for females). These values were all bigger compared to the study by Hwang et al (26) in which they measure 11.7 mm. However, Kazkayasi et al (18) and Rahman et al (19) measured 22.95 mm and 13 mm. The mean length of the IOG was found to be 3.52 ± 0.97 mm on the right side and 3.46 ± 0.79 mm on the left side in the present study. This was different from the 16.7-mm length found by Hwang et al (26), the 5.95-mm length found by Kazayasi et al (18) and the 14-mm length found by Rahman et al (19). These different measurements of the IOG and the IOC may be due to their definitions. In the present study, the IOC was identified as the distance from the IOF to the portion covered by the bone of the orbital floor.

Previous studies reported that the supraorbital notch (foramen), midline, infraorbital rim and ANS were taken as reference points for the determination of the location of the IOF (15, 16, 18, 27). Chung et al (16), stated that the IOF was 27.2 mm lateral to the midline in Koreans. Hwang et al (26) indicated that the distance of the IOF from the midline was 26.5 mm. Similarly, the IOF was approximately 25.7 mm (26.5 mm in males, 25.08 mm in females) lateral to the midline in this study. Chrcanovic et al (28) reported that the mean location of the IOF was 6.5 mm inferior of the inferior orbital rim compared to the 9.6-mm measured by Hwang et al (26) and to our study, which found 7.43 mm on the right side and 7.66 mm on the left side. The discrepancy in the measurement may again be due to the definition of the reference point: the upper pole of the IOF was taken as the reference point for the measurement. Because the measurements may vary considerably among ethnicities and individuals, we aimed to locate the IOF with less variability from the surrounding structures more conveniently in living subjects by using the ANS as a reference point.

Regarding the oval or rounded shape of the IOF, although most of the foramen are oval, we found no statistically significant difference (Tab. I). Singh (29) reported 3 different shapes of infraorbital foramen, i.e., vertical oval, horizontal oval and circular, but he also reported that most of them were vertical oval. In the present study, the change in the shape of infraorbital foramen was also examined, but no statistically significant difference was observed between the age groups regarding the oval or round shape of the optic canal and the IOF according to age groups (Tab. V). Previous studies stated that the location of the IOF changes by age (5, 30). Facial bones show rapid growth from ages 3 to 4 years, and the orbit was found to attain maturity at the age of 16 years (31, 32). Lee et al (5) also reported that the mean distance between dacryon-IOF and IOF-IOM was stabilized after 20 years. In the present study no statistically significant difference was observed between young and older subjects (Tab. IV). It is noted than our study population only comprises people between 18 and 70 years old, which means that the growth in the youngest group (18-25 years old) was already completed, resulting in no significant difference. In addition, the lengths of the ANS-NB, FR-FR, FR-IOF, IOF-IOF, N-ANS, S-FR, S-N, S-cIOF, cIOF-N , InfOF-IOF, InfOF-IOM, cIOF-CT, cIOF-NB, IOC and IOG were all significantly greater in males (Tab. III). In all cases the average of the IOC length on the right side was determined to be significantly longer compared to the left side ($p = 0.029$; $p<0.05$) (Tab. III). In all males, the average length of the IOC on the right side was found to be longer compared to the left side (Tab. III).

Conclusions

In conclusion, it may be stated that the size of the IOF and the distance between the IOF and most of the anatomical points differ between sexes. These results provide detailed knowledge of the anatomical characteristics in this particular area. CBCT imaging with lower radiation doses and in thin slices can be a powerful tool prior to any surgical approach and for generating artificial prostheses.

Disclosures

Financial support: No grants or funding have been received for this study.
Conflicts of interest: None of the authors has financial interest related to this study to disclose.

References

1. Sharma N, De M, Pracy P. Recurrent facial paraesthesia secondary to maxillary antral cyst and dehiscent infraorbital canal: case report. J Laryngol Otol. 2007;121(06):e6.
2. Abed SF, Shams PN, Shen S, Adds PJ, Uddin JM. Morphometric and geometric anatomy of the caucasian orbital floor. Orbit. 2011;30(5):214-220.
3. Gray H, Clemente CD, eds. Gray's Anatomy of the Human Body. Baltimore, MD: Williams and Wilkins 2008.
4. Suresh S, Patel AS, Dunham ME, et al. A randomized double-blind controlled trial of infraorbital nerve block versus intravenous morphine sulfate for children undergoing endoscopic sinus surgery: are postoperative outcomes different? Anesthesiology. 2002;96:A1292.
5. Lee T, Lee H, Baek S. A three-dimensional computed tomographic measurement of the location of infraorbital foramen in East Asians. J Craniofac Surg. 2012;23(4):1169-1173.
6. Schultze-Mosgau S, Krems H, Ott R, Neukam FW. A prospective electromyographic and computer-aided thermal sensitivity assessment of nerve lesions after sagittal split osteotomy and Le Fort I osteotomy. J Oral Maxillofac Surg. 2001;59(2):128-138, discussion 138-139.
7. Mozzo P, Procacci C, Tacconi A, Martini PT, Andreis IA. A new volumetric CT machine for dental imaging based on the cone-beam technique: preliminary results. Eur Radiol. 1998;8(9):1558-1564.
8. Brown AA, Scarfe WC, Scheetz JP, Silveira AM, Farman AG. Linear accuracy of cone beam CT derived 3D images. Angle Orthod. 2009;79(1):150-157.
9. Oz U, Orhan K, Abe N. Comparison of linear and angular measurements using two-dimensional conventional methods and three-dimensional cone beam CT images reconstructed from a volumetric rendering program *in vivo*. Dentomaxillofac Radiol. 2011;40(8):492-500.
10. Hwang SH, Seo JH, Joo YH, Kim BG, Cho JH, Kang JM. An anatomic study using three-dimensional reconstruction for pterygopalatine fossa infiltration via the greater palatine canal. Clin Anat. 2011;24(5):576-582.
11. Kalender A, Orhan K, Aksoy U. Evaluation of the mental foramen and accessory mental foramen in Turkish patients using cone-beam computed tomography images reconstructed from a volumetric rendering program. Clin Anat. 2012;25(5): 584-592.

12. Liang X, Jacobs R, Hassan B, et al. A comparative evaluation of Cone Beam Computed Tomography (CBCT) and Multi-Slice CT (MSCT) Part I. On subjective image quality. Eur J Radiol. 2010;75(2):265-269.
13. Cevidanes LH, Hajati AK, Paniagua B, et al. Quantification of condylar resorption in temporomandibular joint osteoarthritis. Oral Surg Oral Med Oral Pathol Oral Radiol Endod. 2010;110(1):110-117.
14. Gomes LR, Gomes MR, Gonçalves JR, et al. Cone beam computed tomography-based models versus multislice spiral computed tomography-based models for assessing condylar morphology. Oral Surg Oral Med Oral Pathol Oral Radiol. 2016;121(1):96-105.
15. Boopathi S, Chakravarthy Marx S, Dhalapathy SL, Anupa S. Anthropometric analysis of the infraorbital foramen in a South Indian population. Singapore Med J. 2010;51(9):730-735
16. Chung MS, Kim HJ, Kang HS, Chung IH. Locational relationship of the supraorbital notch or foramen and infraorbital and mental foramina in Koreans. Acta Anat (Basel). 1995;154(2): 162-166.
17. Gupta T. Localization of important facial foramina encountered in maxillo-facial surgery. Clin Anat. 2008;21(7):633-640.
18. Kazkayasi M, Ergin A, Ersoy M, Bengi O, Tekdemir I, Elhan A. Certain anatomical relations and the precise morphometry of the infraorbital foramen—canal and groove: an anatomical and cephalometric study. Laryngoscope. 2001;111(4):609-614.
19. Rahman M, Richter EO, Osawa S, Rhoton AL Jr. Anatomic study of the infraorbital foramen for radiofrequency neurotomy of the infraorbital nerve. Neurosurgery. 2009;64(5)(Suppl 2): 423-427, discussion 427-428.
20. Ludlow JB, Ivanovic M. Comparative dosimetry of dental CBCT devices and 64-slice CT for oral and maxillofacial radiology. Oral Surg Oral Med Oral Pathol Oral Radiol Endod. 2008;106(1): 106-114.
21. Periago DR, Scarfe WC, Moshiri M, Scheetz JP, Silveira AM, Farman AG. Linear accuracy and reliability of cone beam CT derived 3-dimensional images constructed using an orthodontic volumetric rendering program. Angle Orthod. 2008;78(3): 387-395.
22. Alexiou K, Stamatakis H, Tsiklakis K. Evaluation of the severity of temporomandibular joint osteoarthritic changes related to age using cone beam computed tomography. Dentomaxillofac Radiol. 2009;38(3):141-147.
23. Ji Y, Qian Z, Dong Y, Zhou H, Fan X. Quantitative morphometry of the orbit in Chinese adults based on a three-dimensional reconstruction method. J Anat. 2010;217(5):501-506.
24. Aggarwal A, Kaur H, Gupta T, et al. Anatomical study of the infraorbital foramen: A basis for successful infraorbital nerve block. Clin Anat. 2015;28(6):753-760.
25. Lee UY, Nam SH, Han SH, Choi KN, Kim TJ. Morphological characteristics of the infraorbital foramen and infraorbital canal using three-dimensional models. Surg Radiol Anat. 2006;28(2): 115-120.
26. Hwang SH, Kim SW, Park CS, Kim SW, Cho JH, Kang JM. Morphometric analysis of the infraorbital groove, canal, and foramen on three-dimensional reconstruction of computed tomography scans. Surg Radiol Anat. 2013;35(7):565-571.
27. Agthong S, Huanmanop T, Chentanez V. Anatomical variations of the supraorbital, infraorbital, and mental foramina related to gender and side. J Oral Maxillofac Surg. 2005;63(6):800-804.
28. Chrcanovic BR, Abreu MH, Custódio AL. A morphometric analysis of supraorbital and infraorbital foramina relative to surgical landmarks. Surg Radiol Anat. 2011;33(4):329-335.
29. Singh R. Morphometric analysis of infraorbital foramen in Indian dry skulls. Anat Cell Biol. 2011;44(1):79-83.
30. Suresh S, Voronov P, Curran J. Infraorbital nerve block in children: a computerized tomographic measurement of the location of the infraorbital foramen. Reg Anesth Pain Med. 2006; 31(3):211-214.
31. Enlow DH. Facial Growth. 3rd ed. Philadelphia, PA: WB Saunders Company 1990.
32. Schumacher GH. Principles of skeletal growth. In: Dixon A, Hoyte D, Ronning O, eds. Fundamentals of Craniofacial Growth. Boca Raton, FL: CRC Press 1997;1-21.